ResearchGate

See discussions, stats, and author profiles for this publication at: https://www.researchgate.net/publication/321419229

Metal Oxide Resistive Switching Memory: Materials, Properties, and Switching Mechanisms

Article *in* Ceramics International · May 2017

CITATIONS
26

READS
6,043

4 authors, including:

Dayanand Kumar
King Abdullah University of Science and Technology
45 PUBLICATIONS **570** CITATIONS
SEE PROFILE

Rakesh Aluguri
36 PUBLICATIONS **671** CITATIONS
SEE PROFILE

All content following this page was uploaded by Dayanand Kumar on 05 December 2017.

The user has requested enhancement of the downloaded file.

Ceramics International 43 (2017) S547–S556

Contents lists available at ScienceDirect

Ceramics International

journal homepage: www.elsevier.com/locate/ceramint

Metal oxide resistive switching memory: Materials, properties and switching mechanisms

D. Kumar, R. Aluguri, U. Chand, T.Y. Tseng*

Department of Electronics Engineering and Institute of Electronics, National Chiao Tung University, Hsinchu 30010, Taiwan

ARTICLE INFO

Keywords:
RRAM
Conduction mechanism

ABSTRACT

With the continuously changing landscape of the computer technologies, a new memory type is needed that will be fast, energy efficient and long-lasting. It shall combine the speed of random access memory (RAM) and non-volatile in the same time. Resistive RAM (RRAM) is one of the most promising candidates in this respect. RRAM has attracted a great deal of attention owing to its potential as a possible replacement for flash memory in next-generation nonvolatile memory (NVM) applications. A brief summary of binary metal oxide RRAM is given in this review. We discuss the RRAM technology development based on published papers, including the mechanism of resistive switching in transition metal oxides, resistive switching materials, device structure, properties, and reliability such as endurance and retention of the device. We also provide possible solutions through innovations in device materials, structures, and understanding the device physics.

1. Introduction

Along with logic integrated circuits (ICs), the memory ICs form major portion of semiconductor device production. Non-volatile memory (NVM) devices are reportedly increasing interest for modern microprocessor-based devices which run a variety of functions within computer, cars, mobile phones, digital cameras, portable electronic gadgets and other so many wireless products. Current nonvolatile memory technology, flash memory, is based on charge storage and this technology is rapidly reaching its physical limits. Therefore, non-charge based nano-scale memories are being intensively studied for next generation nonvolatile memory applications, such as ferroelectric RAM (FeRAM), magnetic random access memory (MRAM), phase change random access memory (PCRAM), and resistive random access memory (RRAM). Among all of the emerging technologies, RRAM is one of the most promising candidates, due to its simple constituents, high density, low power, large endurance, fast write, read and erase speeds and excellent scalability as shown in Table 1. The device structure is simple capacitor-like metal-insulator-metal (MIM) structure as shown in Fig. 1a. On the application of a proper electrical signal, the resistance of the MIM structure can be switched from one state to other and the structure retains current resistance state until an appropriate electrical signal is applied to change it, representing its non-volatile nature. Recent work on the oxide based resistive switching memory can be traced back to the discovery of hysteresis I-V characteristics in perovskite oxides such as $Pr_{0.7}Ca_{0.3}MnO_3$ [1,2], $SrZrO_3$ [3], $SrTiO_3$ [4], etc. in the late 1990s and the early 2000s. Since Samsung demonstrated NiO memory array integrated with the 0.18 μm silicon CMOS technology in 2004 [5], research activities have been focused on binary oxides such as NiOx [6], TiOx [7], CuOx [8], ZrOx [9], ZnOx [10], HfOx [11], TaOx [12], AlOx [13], etc., because of the simplicity of the material and good compatibility with silicon CMOS fabrication process. There are different types of memory devices based on the selector used/not used in it like one transistor one resistor, one diode one resistor and complementary resistor switch, etc [14]. To be precise, the schematic and circuit diagram of the resistive memory device with a one-transistor-one-resistor (1T1R) structure is shown in Fig. 2. Here each resistor in the cross bar array works as a storage element and each transistor is used to select the particular storage node to be accessed and reduces the sneak path current problem.

Investigation of the resistance switching behavior in various types of materials and structures attracts broad interest about its memory application from 2004 to present. Among those resistive-switching materials, binary metal oxides are the most promising for practical applications because their compatibility with CMOS BEOL processing. Therefore, RRAM reveals high potential being a main NVM device to possibly replace the currently flash memory in the future. In this review, we focus on the binary metal–oxides RRAM and review their projected resistance switching mechanisms, materials belongings and device characteristics, and key routine metrics and their device scaling

* Corresponding author.
E-mail address: tseng@cc.nctu.edu.tw (T.Y. Tseng).

http://dx.doi.org/10.1016/j.ceramint.2017.05.289

Available online 31 May 2017
0272-8842/ © 2017 Elsevier Ltd and Techna Group S.r.l. All rights reserved.

Table 1
Comparison between the properties of various recent non-volatile memory devices.

	DRAM	PCRAM	RRAM	MRAM	FRAM
Non-Volatile	No	Yes	Yes	Yes	Yes
Technology node	3x nm	4x nm	5x nm	130 nm	180 nm
Granularity	Small	Small	Small	Small	Large
Software	Easy	Easy	Easy	Easy	Easy
Write Operation Voltage (V)	2.5	3	3	1.8	0.6
Write Time	< 10 ns	50 ns	< 5 ns	< 100 ns	20 ns
Erase Time	< 10 ns	120 ns	< 5 ns	< 100 ns	20 ns
Read Time	< 10 ns	< 60 ns	< 10 ns	< 20 ns	20 ns
Endurance	> 3E16	1E15	1E12	> 3E16	1E14

trends. We have chosen interesting material high –k HfO_2 and review it in more detail. Besides, we discussed future outlook for RRAM and its emerging applications for reconfigurable logic and neuromorphic computing.

2. Operation principle of RRAM

Generally speaking, there are two types of resistive switching memory. One type is based on the conductive filaments (CF) of oxygen vacancies (Vo); the other type is based on the CF of metal atoms, which is also called conductive-bridge RAM (CBRAM). CBRAM relies on the fast-diffusive Ag or Cu ions migration into the oxide (or chalcogenide) to form a conductive bridge [15,16]. Fig. 1 shows the schematic diagrams of the transition metal oxide (TMO) resistive memory device with its switching I-V curves [17]. We first introduce some basic concepts and terminologies about metal–oxide RRAM. The operation principle of RRAM is based on the reversible resistive switching (RS) between at least two stable resistance states, the high resistance state (HRS) and low resistance state (LRS), which occurs in TMO in simple metal-insulator-metal (MIM) configurations as shown in Fig. 1. There exist two types of the switching memory associated with the electrical polarity requisite for the switching properties. In general, the operation which changes the resistance of the device from high resistance state (HRS) to low resistance state (LRS) is called SET process, while the opposite process is defined as RESET. The specific resistance state (HRS or LRS) can be retained after the electric stress is cancelled, which indicates the nonvolatile nature of RRAM. Usually for the fresh samples in their initial resistance state, a voltage larger than the set voltage is needed to trigger on the resistive switching behaviors for the subsequent cycles. This is called the forming process or electroforming. Based on the relationship of electrical polarity between SET and RESET processes, the resistive switching behaviors can be divided into two modes: unipolar and bipolar as shown in Fig. 1. In the unipolar RRAM, the switching direction does not depend on the polarity of the applied voltage but depends on the amplitude of the applied voltage as indicated in Fig. 1b. The device switches from HRS to LRS occurs under the same voltage polarity as the switching from LRS to HRS. If the unipolar switching can symmetrically occurs at both positive and negative voltages, it is referred to the nonpolar switching behavior. In the bipolar RRAM, switching direction depends on the polarity of applied voltage as shown in Fig. 1c. Thus, writing and erasing occur under the different polarity. For the each switching mode, in order to avoid the permanent dielectric breakdown in the set process, it is recommended to enforce to set compliance, which is usually provided by the memory cell transistor, series resistor or semiconductor parameter analyzer. To read the data from the memory cell, a small voltage is applied that does not affect the memory cell to detect whether the cell is in LRS or HRS.

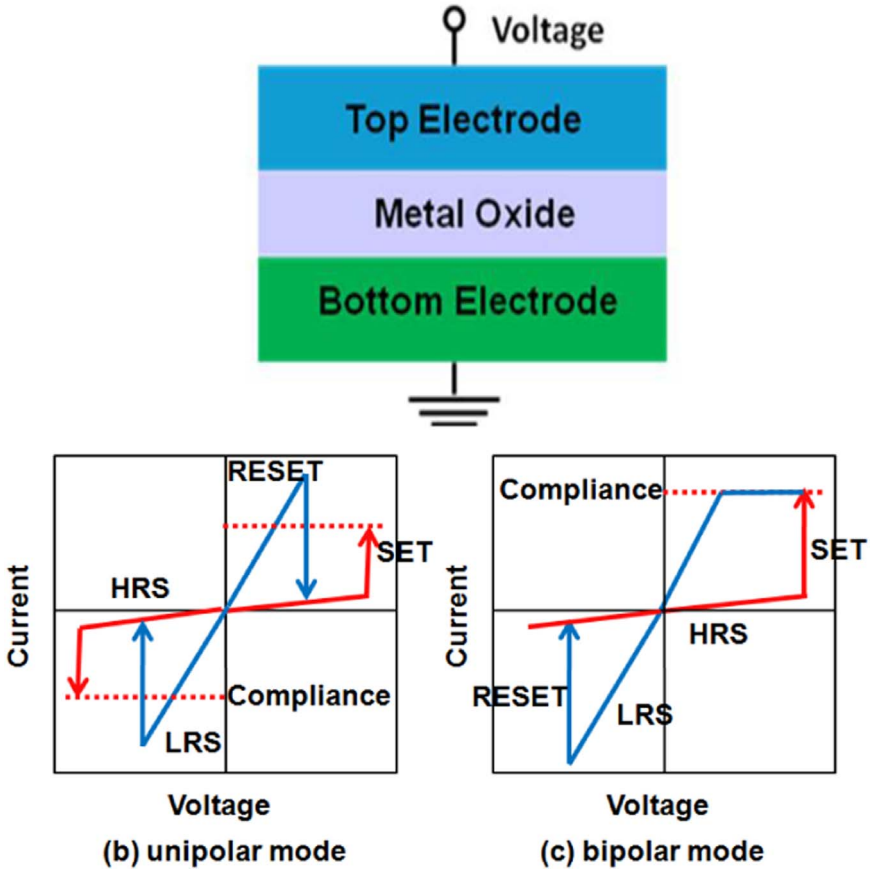

Fig. 1. (a) Schematic of metal-insulator-metal structure for oxide RRAM, and schematic of metal oxide memory's I-V curves, showing two modes of operation: (b) unipolar and (c) bipolar [17].

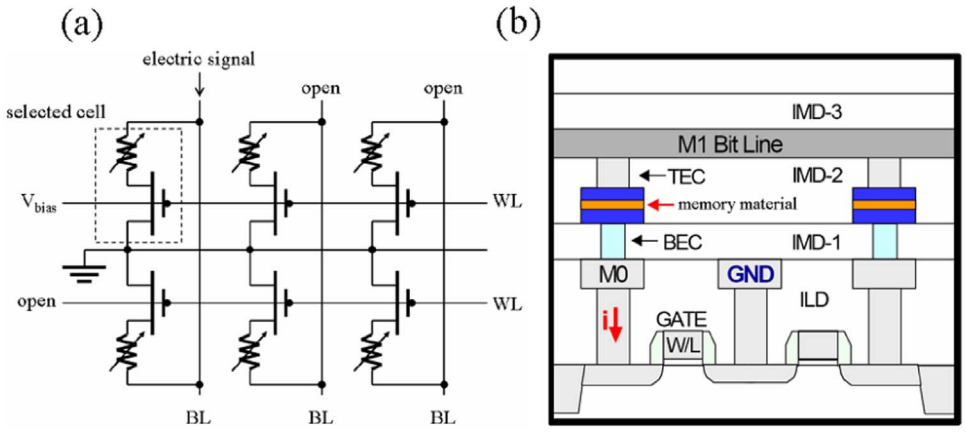

Fig. 2. (a) Basic circuit diagram of the 1T1R structure of RRAM. (b) Cross section view schematic diagram of the 1T1R structure of RRAM.

3. Resistive switching mechanisms

To understand the mechanism in the RRAM devices, we introduce the classification of switching mechanisms. Generally speaking, there are three types of RRAM devices based on the switching mechanism undergoing in the device. The first type is based on the conductive filaments consisting of oxygen vacancies, which are typically referred to as oxide-based RRAM. The second type is based on the conductive filaments consisting of metal atoms, which is called CBRAM. The third type is based on the charge trapping/detrapping within the device, which is called electronic mechanism.

3.1. Oxygen ions migration

Most of resistive switching behaviors are caused by the oxygen ions migration between the electrodes, that is, the resistive switching layer, leading to form conduction filament [18]. The schematic diagram of switching process depicts the oxygen ions migrated and diffused as shown in Fig. 3. During the forming process, soft dielectric breakdown occurs and oxygen ions drift to the anode interface by the high electric field, where they are discharged as neutral non-lattice oxygen if the anode materials are noble metals or react with the oxidizable anode materials to form an interfacial oxide layer. Thus, the electrode/oxide interface behaves like an oxygen reservoir [19]. For a memory cell in the LRS, the current flows through the CFs in the bulk oxide. During the reset process, oxygen ions migrate back to the bulk to recombine with the oxygen vacancies and return the memory cell to the HRS.

3.2. Metal Ion migration

In particular, for the solid-state electrolyte, when one involved electrode metal is situated in the intermediate range of the electrochemical potential series and forms mobile cations, such as Ag^+ and Cu^+, bipolar resistive switching characteristics are observed, and

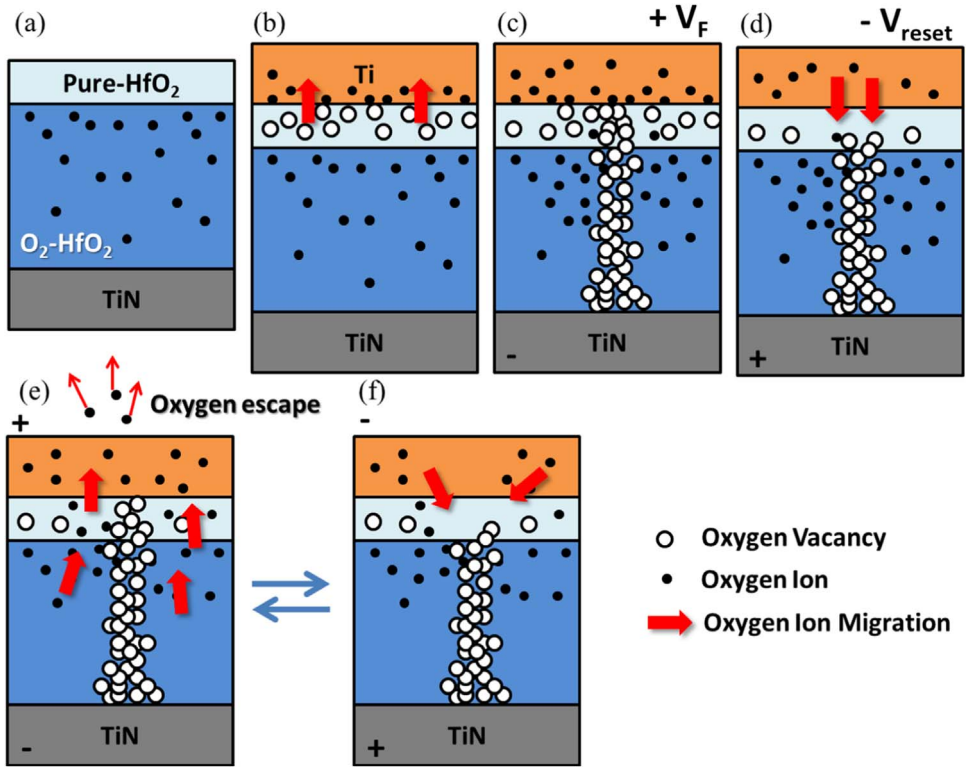

Fig. 3. Schematic description of the RS mechanism of the device. (a) Before and (b) after the Ti top electrode deposition. (c) CF grows from TiN to Ti electrodes under a positive forming voltage on it. (d) A negative voltage is applied on it for rupture the CF. (e) CF formation and some oxygen ions release during set process. (f) CF ruptures during reset process. [19].

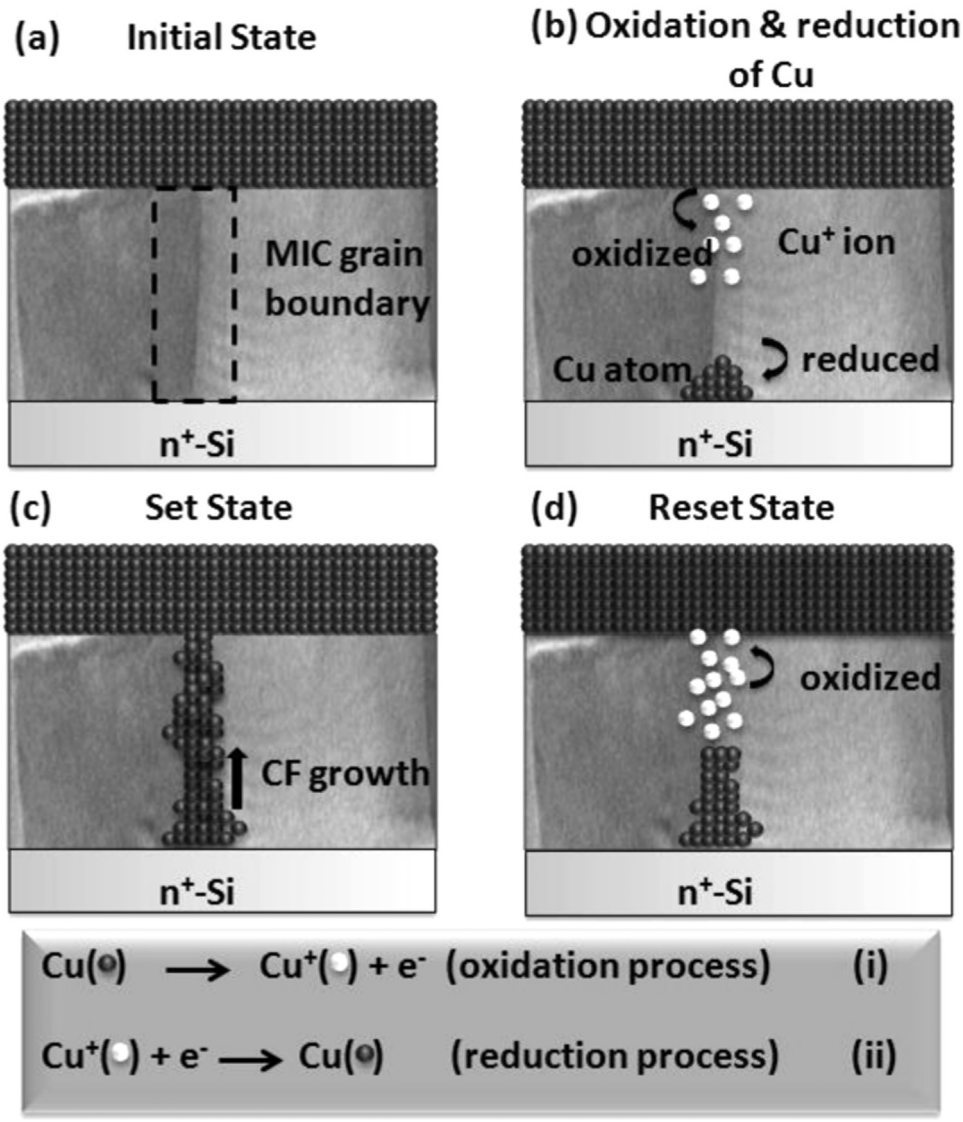

Fig. 4. Sketch of a resistive switching effect based on the electrochemical metallization process [20].

electrochemical redox processes are generally accepted to be responsible for the resistive switching. Here, the set process is owing to the electrochemical formation of metallic filaments in the ion-conducting electrolyte, whereas the reset process is triggered by the dissolution of these metallic filaments.

The RS mechanism of the demonstrated devices is schematically illustrated in Fig. 4. [20]. When a positive voltage is applied on the Cu top electrode, oxidation occurs on this electrochemically active material. Therefore, Cu+ cations are generated as shown in Fig. 4b. The mobile Cu^{+} cations migrate toward bottom electrode along the metal induced crystallization (MIC) grain boundary and are deoxidized back to Cu metal atoms. The successive Cu metal atoms accumulated at bottom electrode start to form a bridge connecting the bottom electrode and the top electrode in the poly-Si layer. Finally, the CF grows between the top and bottom electrodes, and then the device changes from HRS to LRS or ON-state as shown in Fig. 4c. The Cu+ cations can easily migrate along the grain boundaries in poly-Si RS layer under an external applied voltage. When a negative voltage is applied on the top electrode during the reset process, the Cu metal ion can easily drift along MIC region of poly-Si thin film to the top of the CF and the oxidation happens to dissolve the filament. Therefore, the conductive filament is ruptured and the device switches from LRS to HRS, as depicted in Fig. 4d.

3.3. Electronic mechanism

Generally, in most cases, conductive filaments are formed as a result of ion migration and redox processes. However, there have been reports on additional class of devices, in which resistive switching is considered to be based on electronic mechanism. The resistive switching device based on a pure electronic mechanism is the charge trapping/detrapping based devices.

Odagawa et al. reported that the Pt/PCMO/Ag RRAM devices have shown that its resistive switching was belonging to trapping and detrapping of carriers (holes), due to the currents of the PCMO-based devices follow the trap-controlled SCLC conduction mechanism [21]. This type of resistive switching mechanism caused by trapping and detrapping of trap states, and changes in valences, is defined as charge transfer. The collective nature in the trap-filling and trap-defilling processes due to strong electron correlation may play a key role in the resistive switching phenomenon.

Metal–Insulator-Transition (MIT) is another form of electronic effect that can lead to resistive switching especially in certain strongly correlated materials such as VO_2, NbO_2 etc. MIT is characterized by a fast, reversible transition between a low resistive metallic state and high resistive insulating state of an oxide [22].

4. Resistive switching materials

A basic structure of the RRAM device is a combination of metal-insulator-metal (M-I-M), where the insulator often represents the resistive switching thin films. Based on the development of the device structure reported so far, the structure is comprehensively separated into bottom electrode, resistive switching layer (RSL) and top electrode.

4.1. Resistive switching layer

The binary metal oxides including NiO, ZnO, CoO, MgO, TiO_2, ZrO_2, HfO_2, CeO_2, Cu_2O, Al_2O_3, Fe_2O_3, Nb_2O_5, Ta_2O_5, Nb_2O_5, WOx, MoOx, etc are used as RSL. The complex metal oxide materials such as $Bi_4Ti_3O_{12}$, $Ba_{0.7}Sr_{0.3}TiO_3$, (Ba,Sr)(Zr,Ti)O_3, $SrTiO_3$, $SrZrO_3$, $LiNbO_3$, $PbTiO_3$, $PbZr_{0.2}Ti_{0.8}O_3$, and the carrier-doped manganites with the perovskite structure, $R_{1-x}A_xMnO_3$ (where R and A are rare and alkaline-earth ions, respectively), including $Pr_{1-x}Ca_xMnO_3$, $La_{1-x}Ca_xMnO_3$, $La_{1-x}Sr_xMnO_3$, and $Nd_{0.7}Ca_{0.3}MnO_3$ play a role of RSL.

4.2. Bottom electrode

The bottom electrode, exhibits the effects of the work function, electronegativity, oxygen affinity, interface reaction, and interdiffusion. Noble metals such as Pt, Au, and Ru, and Ti, TiN, TaN, usually serve as the bottom electrodes. Yang et al. used the Cu_2O film with Pt top electrode combining with various bottom electrodes to investigate their effects on the RS properties [23]. It was elucidated that only when Ohmic or low Schottky contact is formed to create enough electric field across the Cu_2O film to induce the resistive switching behavior. The active materials such as TiN, Ti, Al also work as the bottom electrodes and modulate the resistive switching behavior via formation of an interface layer near the switching layer, where function as an oxygen reservoir leading to the formation/rupture of the conducting filaments near the interface. However, the active bottom electrode faces a serious thermal budget issue because that the following high temperature process may lead to the excessive reaction between the bottom electrode and RSL.

4.3. Top electrode

Many reports about the research on the effect of top electrode on the RS behaviors of RRAM have been proposed. Sawa et al. proposed that a Schottky barrier, the origin of the nonlinearity of the current-voltage (I-V) curve, was formed by a low work function metal and a p-type semiconductor $Pr_{0.7}Ca_{0.3}MnO_3$, and the RS mechanism based on Schottky barrier modulation was suggested [24]. Afterward, Kim et al. and Sim et al. came to the similar conclusion by observing the RS phenomena in the $Pr_{1-x}Ca_xMnO_3$ and in the Nb:$SrTiO_3$ films, respectively as well [25,26]. Oppositely, Seo et al. demonstrated that the effective electric field across the NiO film was high enough to cause resistive switching phenomenon while Ohmic contact or a low Schottky barrier formed between the M-I and I-M interfaces [27]. There was no resistive switching phenomenon with Ti top electrode due to the considerable voltage drop across the well-established Schottky barrier at the Ti/NiO interface. Fig. 5 depicts that the Au and Pt top electrodes form an Ohmic contact with the NiO films, and thus, the capacitance values increase linearly with the absolute value of voltage sweeping [27]. Therefore, the resistive switching in these devices is due to the high effective electric field induced in the NiO films that causes carrier trapping/detrapping at the defect states. For Al/NiO/Pt device, a low schottky barrier is formed at Al/NiO interface causing the resistive switching at higher voltages. For Ti/NiO/Pt device, the voltage drop at the Ti/NiO interface is large enough causing the effective electric field

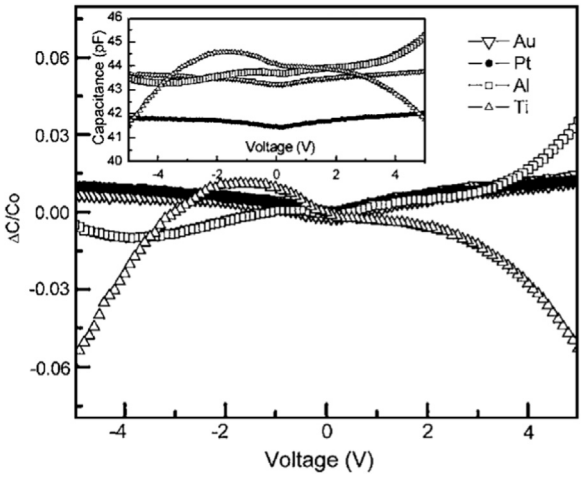

Fig. 5. Modified capacitance change $(C-C_0)/C_0$ in Au/NiO/Pt, Pt/NiO/Pt, Al/NiO/Pt, and Ti/NiO/Pt devices as functions of applied voltage bias. The inset shows the measured capacitance-voltage (C-V) curves [27].

inside the NiO film insufficient to persuade resistive switching.

In our previous papers, the ZrO_2-based devices with an active Ti top electrode were demonstrated to exhibit better RS characteristics than those with Al and Pt top electrodes, and a transition from nonpolar to bipolar RS was also observed as shown in Fig. 6 [28,29]. Wang et al., has experimentally investigated that this transition of the RS behavior from nonpolar to bipolar is highly dependent on the thickness of the Ti top electrode [29]. The Ti top electrode was an oxygen-gettering material and easily extracted a large amount of oxygen ions from RSL, further causing the formation of the interface TiO_x/ZrO_y layer. For the thin Ti top electrode (< 20 nm) based devices, the interface layer thickness is very small leading to a negligible series resistance resulting in the device to exhibit nonpolar RS behavior. As the Ti thickness is increased, the oxide deficient TiO_x/ZrO_y interface layer thickness increases and it contributes a countable series resistance to the device, resulting in the devices to exhibit bipolar RS behavior. It is to be noted that the thin Ti top electrode based devices have also exhibited bipolar RS behavior as the interface layer thickness increased after certain cycles of nonpolar RS operation. Therefore, a bipolar resistive switching mechanism was proposed to occur at the region where the formation and rupture of conducting filaments would be confined near the Ti/ZrO_2 interface [9,29]. The effect of Ti top electrode thickness on polarity transition was numerically also studied using Metropolis Monte Carlo algorithm (MMC), in which the enthalpy variation of the resistive switching layer was used to understand the nature of the filament formation and rupture [30]. The RS behavior in these devices is completely dependent on the accumulation and reduction of oxygen vacancies near the Ti/ZrO_2 interface during the forming operation. During forming, a charged interfacial layer with high concentration gradient which induces diffusion current is formed. For the thin Ti top electrode devices this diffusion current is small and not enough to oppose the drift current associated with the applied electric field resulting in the device to exhibit unipolar reset. As the Ti top electrode thickness is increased, the diffusion current increases and after certain thickness, the current attains the value which can oppose the drift current resulting in the device to exhibit bipolar RS behavior [30].

5. Resistive switching properties

A lot of binary metals oxides have been found to exhibit resistive switching behavior. Most of them are transition metal oxides, and some of them are lanthanide series metal oxides which also show resistive

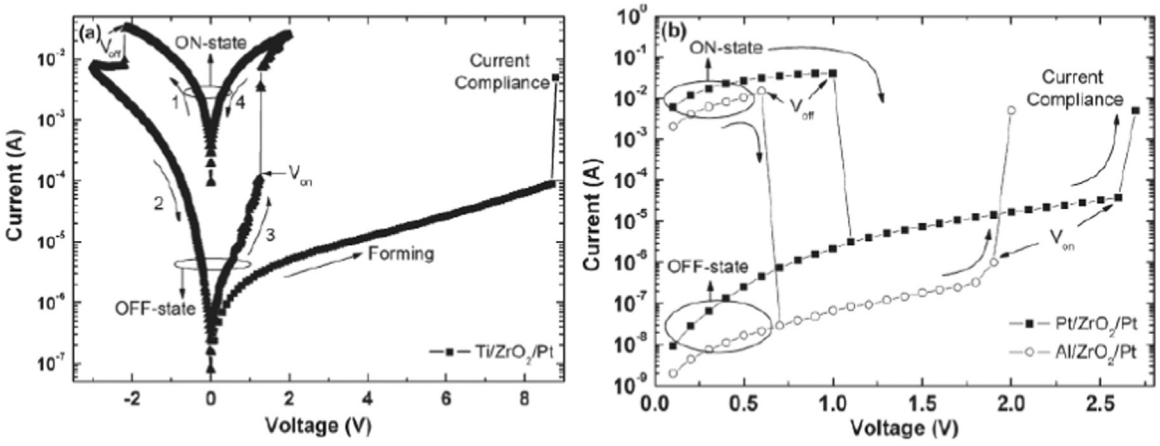

Fig. 6. Typical resistive switching I–V curves of (a) $Ti/ZrO_2/Pt$, (b) $Pt/ZrO_2/Pt$, and $Al/ZrO_2/Pt$ devices, respectively [28].

switching behavior. Here we choose HfO_2, because this has drawn most attention and has been extensively studied in the past several years. Regarding the switching mechanism in HfO_2 devices, most of the reported literature attributes the resistive switching effect to filamentary model. This describes the resistive switching based on the formation and rupture of conducting filaments composed of percolated oxygen vacancies. A widely accepted mechanism is described in Fig. 3.

HfO_2 has attracted extensive attention for its application in RRAM devices which have prospective advantages such as simplicity, low operating power, high speed, and high nonlinearity [11,31,32]. Lee et al. [33], proposed the bipolar resistive switching mechanism of atomic layer deposition (ALD) grown 4-nm-thick HfO_2 films with a $Pt/HfO_2/TiN$ device structure, with the formation and rupture of conducting filaments near the HfO_2/TiN interface. However, by introducing a ZrO_2 layer (by sputter deposition) in the $Pt/HfO_2/TiN$ device to yield a $Pt/ZrO_2/HfO_2/TiN$ structure, unipolar RS behavior was observed, which reveals that the conducting filament formation/rupture within the ZrO_2 layer [33]. A forming voltage of 2.2 V with 10 mA compliance current was used for the forming process. The device was switched on at ~2 V and switched off at ~0.7 V. A 1D1R structure using the $Pt/ZrO_2/HfO_2/TiN$ RRAM device exhibited unipolar switching with higher operation voltages (V_{set} = ~3 V, V_{reset} = ~2 V) with continuous and stable RS behavior, as shown in Fig. 7. Stable retention (> 10^5 s), and nondestructive readout properties were observed for both ON and OFF states at RT and 85 °C.

Gilmer et al., reported HfO_2 based $TiN/HfO_x/Zr/W$ RRAM device with 1T-1R architecture as shown in Fig. 8 [31]. HfO_2 based memory device with bipolar resistive switching behavior shows very low

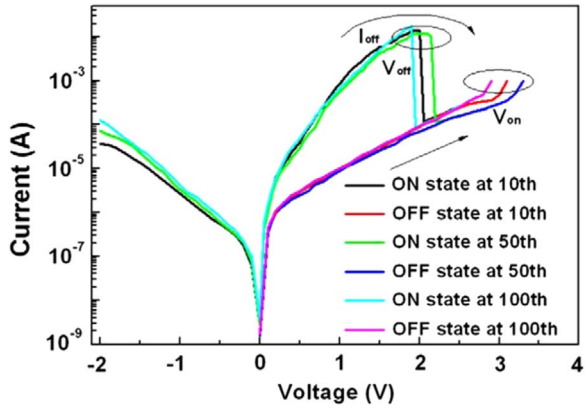

Fig. 7. Unipolar resistive switching characteristics for a $Pt/ZrO_2/HfO_2/TiN$ device in a 1D1R architecture. ON and OFF states are shown after 10, 50, and 100 cycles [33].

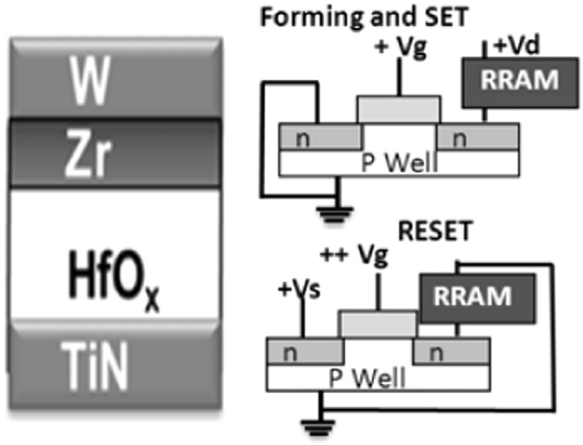

Fig. 8. Schematic of RRAM and 1T1R set-up [31].

operation current I_{compl} (1 μA) and very low operating voltage (± 1 V) for both SET and RESET cases. Both dc and ac measurements were characterized with device size 40 × 40 nm^2 and 7 × 7 μm^2. Good switching speed (80 ns pulses), on/off ratio (> 10) and excellent ac switching endurance up to 10^8 cycles at low power operation for 40 × 40 nm^2 crossbar device.

The highly reliable HfO_2 based device consisting of $TiN/TiO_x/HfO_x/TiN$ structure was fabricated on $Ti/SiO_2/Si$ substrate by post metal annealing (PMA) the $TiN/Ti/HfO_2/TiN$ stack layers. Ti used as a buffer layer to prevent the diffusion of oxygen. A 5 nm HfO_2 film was deposited by ALD and all other films Ti and TiN were deposited by sputter. One transistor and one resistor (1T-1R) configuration was realized by 0.18 μm CMOS technology [11]. The devices were switched at less than 1.5 V for both V_{SET} and V_{RESET} for both 1R and 1T-1R configuration when I_{SET} is larger than 200 μA, as shown in Fig. 9. suggesting that these devices are useful for low voltage application. Adding a Ti thin buffer layer into the top electrode side has resulted in excellent device performances, like low operating current (< 25 μA), higher on/off ratio (> 10^3), excellent switching speed (5 ns), good endurance (> 10^6 cycles) and stable data retention up to 10 years for both R_{LOW} and R_{HIGH} at 200 °C. It is proposed that the Ti acts as oxygen getting material to form interfacial layer, leading to excellent switching properties of HfO_2 [9]. The same group also used AlCu and Ta as the capping layer for the HfO_x memory. These devices also show stable bipolar resistive switching but they have a small on/off ratio about 4 [34], the oxygen capture ability of the capping metal layer may also be responsible for these results.

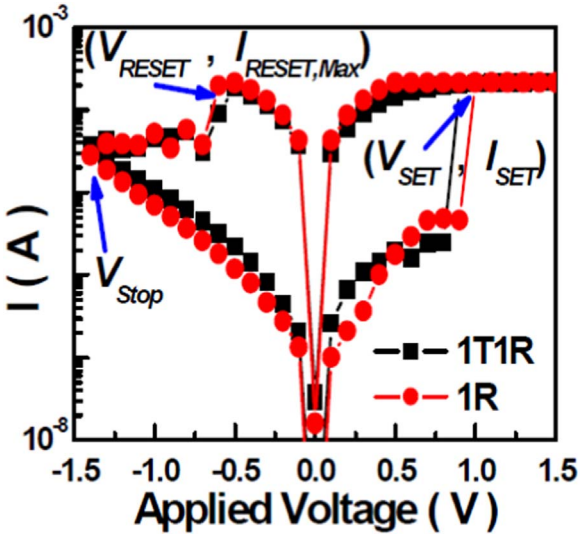

Fig. 9. Comparison of bipolar resistance switching characteristic between the TiN/TiO_x/HfO_x/TiN devices in 1R and 1T1R configuration [11].

The double forming phenomenon was proposed by Huang et al., in TaN/ZrO_2/HfO_2/TiN CMOS compatible structure [35]. In this structure a 5 nm HfO_2 film was deposited by sputter as a first resistive switching (RS) layer at room temperature with 2:1 Ar/O_2 atmosphere of 5 mTorr and 3 nm ZrO_2 was also deposited by sputter as second resistive switching layer with 2:1 Ar/O_2 atmosphere of 10 mTorr. The double forming phenomenon was explained in six steps: (1) First forming process, (2) Medium state, (3) Second forming process, (4) LRS, (5) Reset Process, and (6) HRS as shown in Fig. 10. The conductive filament mechanism with the measured results of X- ray photoelectron spectra (XPS) were employed to explain the double forming phenomenon. It was clearly indicated that the fluctuation of endurance can be improved by controlling the point in the interface between HfO_2 and ZrO_2 films for the formation and rupture of the conductive filament in Fig. 11. Therefore, high endurance (10^7 cycles), large HRS/ LRS ratio (~ 100), good data retention for both LRS and HRS (> 10^4 s) with fast speed (40 ns) were achieved in that structure.

Chand et al., demonstrated high nonlinear resistive switching behavior in the Ti/HfO_2/Al_2O_3/TiN RRAM device with crossbar architecture inserting the Al_2O_3 thin tunnel barrier layer with large band gap [32]. TiN was used as a bottom electrode with the patterning of I- line lithography and high density plasma reactive ion etching process. The 1 or 3 nm thick thin films of Al_2O_3 or TiO_2 as a tunnel barrier layer deposited by ALD and 10 nm HfO_2 also deposited by ALD as a resistive switching layer. The nonlinear resistive switching behavior is shown in Fig. 12. The device with 1 nm thin Al_2O_3 inserting layer depicts the nonlinear resistive switching behavior in Fig. 12a, while the linear resistive switching behavior shows in the TiO_2 as illustrated in Fig. 12b. Such difference attributes to the higher band gap of Al_2O_3 (8.8 eV) with the comparison of TiO_2 (3.5 eV). Therefore, the 1 nm Al_2O_3 inserting layer acts as a tunnel barrier layer in the structure, exhibiting the nonlinear switching characteristics. The nonlinear switching mechanism in the device is caused by Fowler-Nordheim (FN) tunneling rather than by direct tunneling in step (ii) as shown in Fig. 12a, leading to an abrupt increase in current. A high nonlinearity factor 37, good data retention and large endurance more than 10^4 cycles are achieved in Ti/HfO_2/Al_2O_3/TiN device. Walczyk et al., proposed the back-end-of-line (BEOL) integrated 1×1 μm^2 TiN/HfO_2/Ti/TiN device with 1T1R architecture [36]. The dominant conduction process in this device is attributed to the Poole-Frenkel emission mechanism with an O_2 defects based trap level existing below the conduction band edge of the HfO_2. The device shows temperature dependence bipolar resistive switching behavior in the range 213–413 K. The resistance ratio R_{OFF}/R_{ON} decreases with increasing the temperature. This is due to fact that the OFF state current has followed the semiconductor characteristics, whereas the ON state current has associated with a weak metallic like characteristics. This temperature dependence of on state and off state currents has been explained theoretically using Quantum Point Contact (QPC) model. In this model, the off state current variation with temperature is modeled using a temperature dependent confinement potential barrier. According QPC model, off state current flows through a one dimensional filament connecting two electrodes which serves as electron reservoirs. The off state current increases exponentially with both temperature and the potential barrier which is in complete agreement with the experimental data. During the on state, the confinement barrier collapses leading to the current-voltage linear relationship. As the resistance of the layer decreases with increasing temperature based on the effect of temperature coefficient, a small decrease of the on state current with increasing temperature is observed. Thus using QPC model it is found that there is no correlation between the temperature variation of the on state and off state currents.

The performance of the HfO_2 based RRAM devices at low temperature were also investigated for their applications in aerospace and low temperature. Fang et al., has investigated very low temperature (4 K) effect in Pt/HfO_x/TiN RRAM device [37]. The device was

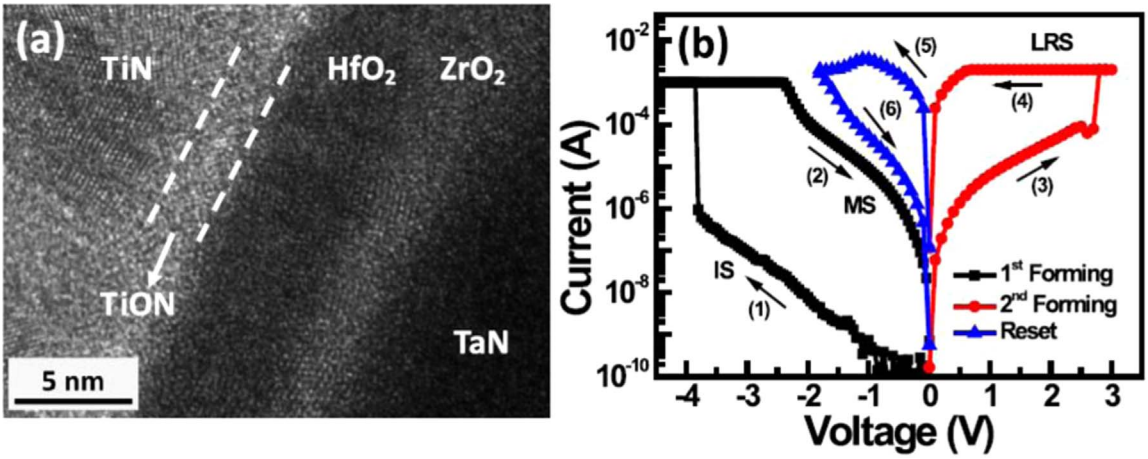

Fig. 10. (a) Typical cross-section TEM image of the TaN/ZrO_2/HfO_2/TiN RRAM device. (b) DC sweep I-V curve of the double forming process phenomenon: (1) First forming process; (2) Medium state; (3) Second forming process; (4) Low resistance state; (5) Reset process; and (6) High resistance state [35].

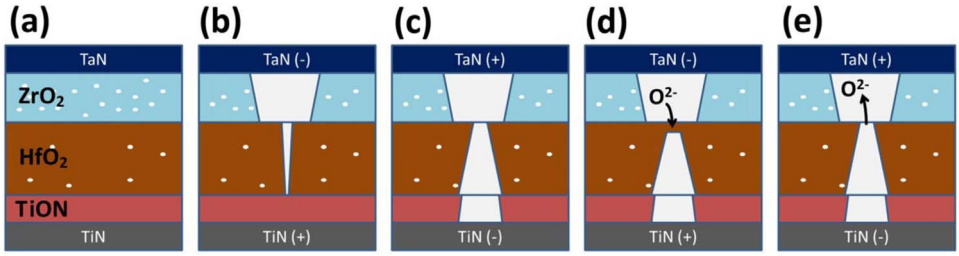

Fig. 11. Schematic description of the conducting mechanism of the double forming process of the TaN/ZrO_2/HfO_2/TiN RRAM device on (a) initial state, (b) first forming process, (c) second forming process, (d) reset process, and (e) set process [35].

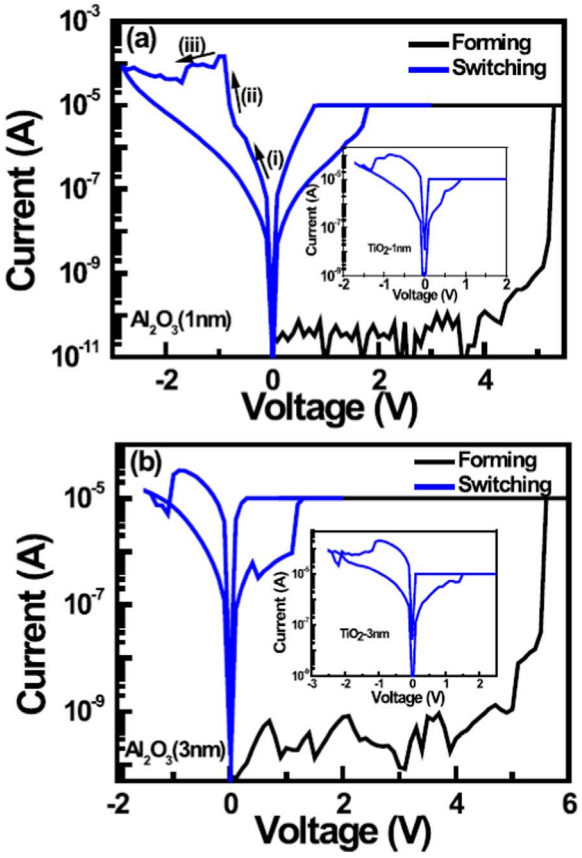

Fig. 12. (a) Forming process and typical *I–V* curves of Ti/HfO_2/(1 nm)Al_2O_3/TiN. Inset: *I–V* curve of Ti/HfO_2/(1 nm)TiO_2/TiN and (b) Forming process and typical *I–V* curves of Ti/HfO_2/(3 nm)Al_2O_3/TiN. Inset: *I–V* curve of Ti/HfO_2/(3 nm)TiO_2/TiN [32].

fabricated in the crossbar structure with an active area of 1 μm^2. The 8 nm HfO_2 as a switching layer was deposited by ALD and 20 nm TiN bottom electrode deposited by sputter by lift-off process with optical lithography on SiO_2/Si substrate. The device exhibited bipolar resistive switching on at ~ 2 V and switched off at ~ 2.5 V. Though, the switching voltage is slightly increased at lower temperature compared with the room temperature, the switching behavior is found to exist up to ultra low temperature of 4 K. As the temperature is decreased, the resistance of the device is increased up to 77 K and followed the nearest neighboring hopping (NNH) conduction mechanism, where the electrons tend to hop to the nearest trap. Below 77 K, the resistance saturates and the thermal energy of the electrons is so small for NNH, tending them to undergo variable range hopping (VRH). The cycle to cycle variation seems to be an inherently stochastic of the RRAM switching dynamics at 4 K.

Tsai et al., investigated the effect of post oxide annealing on the HfO_2 based resistive switching layer at high temperature and O_2 atmosphere in the HfO_2 based crossbar oxygen-ion-based oxide RRAM (OxRRAM) and Cu-ion-based conductive bridge (CBRAM) devices [38]. The 10 nm HfO_2 was deposited by ALD as a switching layer in the Pt/Ti/HfO_2/TiN (OxRRAM) structure and 5 nm HfO_2 was also deposited by ALD as resistive switching layer in Cu/TiW/HfO_2/TiN (CBRAM) structure with crossbar architecture. A 50 nm thick Ti top electrode with 20 nm Pt capping layer was deposited by electron beam evaporation. A 2 nm thick TiW adhesion layer was deposited by electron beam evaporation in CBRAM device. The forming voltages of the devices annealed at 400 and 500 °C in vacuum are largely reduced to 3 V, which is lower than those of devices are annealed in O_2 atmosphere. Due to this switching endurance and device yield (100%) of the CBRAM device are enhanced after post HfO_2 deposition annealing in vacuum. The V_{set} and V_{reset} are reduced in the devices with vacuum annealing due to the generation of considerable amount of oxygen vacancies to ease Cu migration in vacuum annealing. The presence of considerable amount of oxygen vacancies in HfO_2 resistive switching layer in vacuum have been detected by XPS analysis. These

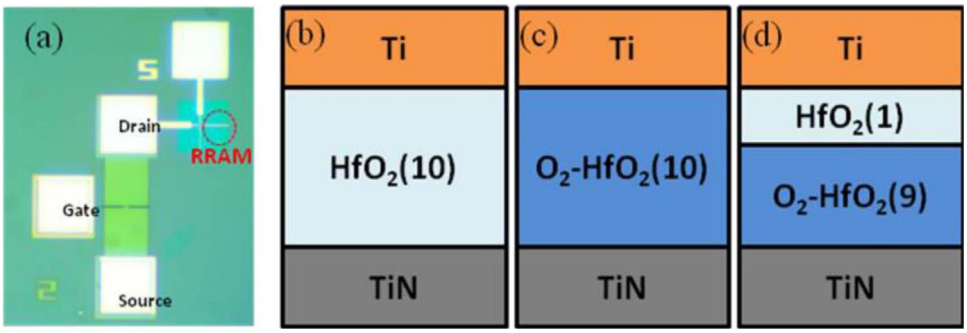

Fig. 13. (a). Optical microscope image of the 1T1R device with cross bar structure. Schematic diagrams of the device structures of (b) Ti/HfO_2(10)/TiN, (c) Ti/O_2- HfO_2(10)/TiN, and (d) Ti/HfO_2(1)/O_2-HfO_2(9)/TiN, respectively [19].

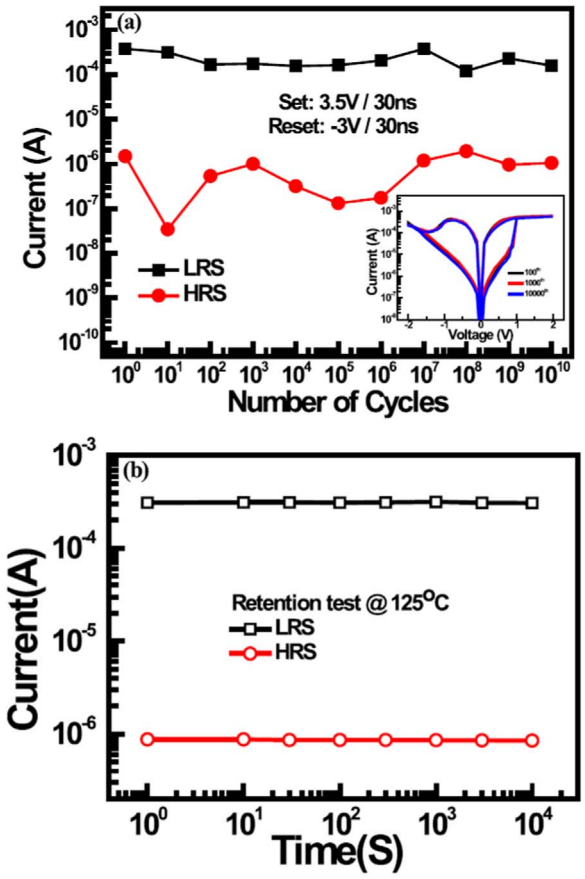

Fig. 14. (a) Dynamic pulse endurance characteristic of the device Ti/HfO_2(1)/O_2-HfO_2(9)/TiN. Inset shows DC sweep curves at 100th, 1000th, and 10,000th cycles (b) Retention test at 125 °C of the same device [19].

oxygen vacancies are responsible for reducing the performance of HfO_2-based OxRRAM device.

Chand et al. [19] used the structures Ti/HfO_2(10)/TiN, Ti/O_2-HfO_2(10)/TiN and Ti/HfO_2(1)/O_2-HfO_2(9)/TiN RRAM with 1T1R configuration. All devices were fabricated at the drain part of the transistor as shown in Fig. 13a. The device Ti/HfO_2(10)/TiN with 10 nm HfO_2 single layer with or without oxygen plasma treatment were fabricated as shown in Fig. 13b. The oxygen plasma treatment can increase the concentration of the oxygen in the 10 nm HfO_2 film as indicated in Fig. 13c. The peak in the interface between O_2-HfO_2 and TiN is caused by the TiN bottom electrode, which is absorbed some part of the oxygen ions. The additional oxygen ions would interstitially exist in the O_2-HfO_2 film. To increase the available number of oxygen ions, the oxygen plasma treatment was applied on the 9 nm HfO_2 layer (O_2-HfO_2) and 1 nm HfO_2 thin layer without the oxygen plasma treatment was deposited to cover such 9 nm HfO_2 film as shown in Fig. 13d. Due to the continuously providing available oxygen ions in 9 nm O_2-HfO_2 layer, the high speed operation (30 ns), high on/off ratio and reliable switching endurance more than 10^1 ° cycles are achieved as shown in Fig. 14a. It needs a high voltage to generate enough energy for constructing the conductive filament during the short pulse time in the AC endurance test [39]. The data retention for the device at 125 °C is shown in Fig. 14b, indicating that both HRS and LRS do not show any degradation in the retention for more than 10^4 s. The comparison between the performances of HfO_2 based memory devices during the recent years has been listed in Table 2.

6. Prospective work

Recent developments in nano-technologies are making available extremely compact and low-power, but also variable and unreliable solid-state devices that can potentially extend the offerings of availing CMOS technologies. It has been demonstrated that the RRAM is a promising candidate for implementing single device based artificial synapses as its resistance depends not only on instantaneous external inputs but also on its past history. One key element that is still a limitation concerns the integration of neurons and synaptic connections in order to realize a brain-like computer. Even though silicon CMOS chips have been designed and fabricated to emulate the brain behaviors, this approach is limited to small systems because it takes several transistors to build an electronic synapse. As the human brain contain more synapses than neurons it is essential to develop a nanoscale, low power, synapse-like device if we want to scale neuromorphic circuits towards the level of the human brain. Therefore, challenge for implementation of neuromorphic computation system is to develop the electronic synapse with ultra-high integration density. Crossbar RRAM array is one of the best solution to this due to their ultra-high integration density. Transition metal oxide based crossbar RRAM reveals high performance memory behavior, such as large endurance, long retention, and low operation voltage. However, there are still some important issues, including the small on/off ratio, large variation during endurance characteristic, operation voltage, device reliability, homogeneity etc., need to be addressed before realizing commercial applications. The unipolar RS behavior with a diode access device is suitable for 3-D ultra-high density stacking memory applications, where each memory cell occupation can be scaled down to an area of only $4f^2$, here, f is the feature size. However, the challenge is that the sneak path leakage of memory arrays without selection device leads to a strong degradation in write/read margin. Large leakage current can further increase the energy consumption in the array. Therefore, the exploration for an ideal selection device for cross-point memory array is one of the most important topics in realizing practical applications of RRAM devices.

Table 2
Recent progress on the performance of HfO_2 based 1T-1R memory devices.

Memristor	TiN/TiO_x/HfO_x/TiN	TiN/TiO_x/HfO_x/TiN	TiN/Hf/HfO_2/TiN	TiN/Ti/HfO_2/TiN	TiN/Ti/HfO_2/TiN	TiN/HfO_x/Zr/W	Ti/HfO_2/O_2-HfO_2/TiN
Structure	1T-1R	1T-1R	1T-1R	1T-1R	1T-1R	1T-1R	1T-1R
Switching Type	Bipolar	Bipolar	Bipolar	Bipolar	Bipolar	Bipolar	Bipolar
Cell Area	180×180 nm^2	30×30 nm^2	10×10 nm^2	–	–	40×40 nm^2	5×5 μm^2
Speed	~5 ns	~0.3 ns	~10 ns	~15 ns	> 10 ns	80 ns	30 ns
Peak Voltage	< 1.5 V	< 2.5 V	< 1.5 V	< 1.3 V	< 1 V	1 V	3.5 V
Peak Current	~25 μA	~200 μA	~50 μA	~275 μA	~275 μA	1 μA	< 1 mA
HRS/LRS Ratio	> 100	> 100	> 10	> 10	> 10	> 10	> 100
Endurance	10^6	10^{10}	5×10^7	10^8	> 10^8	> 10^8	10^{10}
Retention	10^4 s@ 200 °C	10^5 s@ 150 °C	10^5 s@ 200 °C	–	–	–	10^4 s@ 125 °C
References	[30]	[40]	[41]	[42]	[43]	[31]	[19]

Acknowledgement

This work was supported by Ministry of Science and Technology, Taiwan under Contract No. 105-2221-E-009 -143 -MY3.

References

[1] W.W. Zhuang, W. Pan, B.D. Ulrich, J.J. Lee, L. Stecker, A. Burmaster, D.R. Evans, S.T. Hsu, A. Shimaoka, K. Inoue, T. Naka, N.A.K. Sakiyama, Y. Wang, S.Q. Liu, N.J. Wu, A. Ignatiev, Novel colossal magnetoresistive thin film nonvolatile resistance random access memory (RRAM), in: IEEE Int. Electron Devices Meeting (IEDM), 2002, pp. 193–196.

[2] A. Asamitsu, Y. Tomioka, H. Kuwahara, Y. Tokura, Current switching of resistive states in magnetoresistive manganites, Nature 388 (1997) 1995–1997.

[3] A. Beck, J.G. Bednorz, C. Gerber, C. Rossel, D. Widmer, Reproducible switching effect in thin oxide films for memory applications, Appl. Phys. Lett. 77 (2000) 139–141.

[4] Y. Watanabe, J.G. Bednorz, A. Bietsch, C. Gerber, D. Widmer, A. Beck, S.J. Wind, Current-driven insulator–conductor transition and nonvolatile memory in chromium-doped $SrTiO_3$ single crystals, Appl. Phys. Lett. 78 (2001) 3738–3740.

[5] I.G. Baek, M.S. Lee, S. Seo, M.J. Lee, D.H. Seo, D.-S. Suh, J.C. Park, S.O. Park, H.S. Kim, I.K. Yoo, U-In Chung, I.T. Moon, Highly scalable nonvolatile resistive memory using simple binary oxide driven by asymmetric unipolar voltage pulses, in: IEEE Int. Electron Devices Meeting (IEDM), 2004, pp. 587–590.

[6] S. Seo, M.J. Lee, D.H. cSeo, E.J. Jeoung, D.-S. Suh, Y.S. Joung, I.K. Yoo, I.R. Hwang, S.H. Kim, I.S. Byun, J.-S. Kim, J.S. Choi, B.H. Park, Reproducible resistance switching in polycrystalline NiO films, Appl. Phys. Lett. 85 (2004) 5655–5657.

[7] B.J. Choi, D.S. Jeong, S.K. Kim, C. Rohde, S. Choi, J.H. Oh, H.J. Kim, C.S. Hwang, K. Szot, R. Waser, B. Reichenberg, S. Tiedke, Resistive switching mechanism of TiO_2 thin films grown by atomic-layer deposition, J. Appl. Phys. 98 (2005) 033715.

[8] A. Chen, S. Haddad, Y.J. Wu, T. Fang, Z. Lan, S. Avanzino, M. Buynoski, M. Rathor, W.D. Cai, N. Tripsas, C. Bill, M. Vanbuskirk, M. Taguchi, Non- volatile resistive switching for advanced memory applications, in: IEEE Int. Electron Devices Meeting (IEDM), 2005, pp. 746–749.

[9] C.Y. Lin, C.Y. Wu, C.Y. Wu, T.Y. Tseng, C. Hu, Modified resistive switching behavior of ZrO_2 memory films based on the interface layer formed by using Ti top electrode, J. Appl. Phys. 102 (2007) 094101.

[10] N. Xu, L. Liu, X. Sun, X. Liu, D. Han, Y. Wang, R. Han, J. Kang, B. Yu, Characteristics and mechanism of conduction/set process in TiN/ZnO/Pt resistance switching random-access memories, Appl. Phys. Lett. 92 (2008) 232112.

[11] H.Y. Lee, P.S. Chen, T.Y. Wu, Y.S. Chen, C.C. Wang, P.J. Tzeng, C.H. Lin, F. Chen, C.H. Lien, M. Tsai, Low power and high speed bipolar switching with a thin reactive Ti buffer layer in robust HfO_2 based RRAM, in: IEEE Int. Electron Devices Meeting (IEDM), 2008, pp. 297–300.

[12] Z. Wei, Y. Kanzawa, K. Arita, Y. Katoh, K. Kawai, S. Muraoka, S. Mitani, S. Fujii, K. Katayama, M. Iijima, T. Mikawa, T. Ninomiya, R. Miyanaga, Y. Kawashima, K. Tsuji, A. Himeno, T. Okada, R. Azuma, K. Shimakawa, H. Sugaya, T. Takagi, R. Yasuhara, K. Horiba, H. Kumigashira, M. Oshima, Highly reliable TaOx ReRAM and direct evidence of redox reaction mechanism, in: IEEE Int. Electron Devices Meeting (IEDM), 2008, pp. 293–296.

[13] C.Y. Lin, C.Y. Wu, C.Y. Wu, C. Hu, T.Y. Tseng, Bistable resistive switching in Al_2O_3 memory thin films, J. Electrochem. Soc. 154 (2007) 189–192.

[14] R. Aluguri, T.Y. Tseng, Overview of Selector Devices for 3-D Stackable Cross Point RRAM Arrays, IEEE J. Electron. Dev. Soc. 4 (2016) 294–306.

[15] R. Waser, M. Aono, Nanoionics-based resistive switching memories, Nat. Mater. 6 (2007) 833–840.

[16] I. Valov, R. Waser, J.R. Jameson, M.N. Kozicki, Electrochemical metallization memories–fundamentals, applications, prospects, Nanotechnology 22 (2011) 254003.

[17] H.-S.P. Wong, H.-Y. Lee, S. Yu, Y.-S. Chen, Y. Wu, P.-S. Chen, B. Lee, F.T. Chen, M.-J. Tsai, Metal–oxide RRAM, Proc. IEEE 100 (2012) 1951–1970.

[18] S.Y. Wang, T.Y. Tseng, Interface engineering in resistive switching memories, J. Adv. Dielectr. 01 (2011) 141.

[19] U. Chand, C.Y. Huang, J.H. Jieng, W.Y. Jang, C.H. Lin, T.Y. Tseng, Suppression of endurance degradation by utilizing oxygen plasma treatment in HfO_2 resistive switching memory, Appl. Phys. Lett. 106 (2015) 153502.

[20] U. Chand, C.Y. Huang, D. Kumar, T.Y. Tseng, Metal induced crystallized poly-Si-based conductive bridge resistive switching memory device with one transistor and one resistor architecture, Appl. Phys. Lett. 107 (2015) 203502.

[21] A. Odagawa, H. Sato, I.H. Inoue, H. Akoh, M. Kawasaki, Y. Tokura, Colossal electroresistance of a $Pr_{0.7}Ca_{0.3}MnO_3$ thin film at room temperature, Phys. Rev. B 70 (2004) 224403.

[22] M. Imada, A. Fujimori, Y. Tokura, Metal-insulator transitions, Rev. Mod. Phys. 70 (1998) 1039.

[23] W.Y. Yang, S.W. Rhee, Effect of electrode material on the resistance switching of Cu_2O film, Appl. Phys. Lett. 91 (2007) 232907.

[24] A. Sawa, T. Fujii, M. Kawasaki, Y. Tokura, Interface transport properties and resistance switching in perovskite-oxide heterojunctions, Proc. SPIE 59322C (2005).

[25] C.J. Kim, I.W. Chen, Effect of top electrode on resistance switching of $(Pr,Ca)MnO_3$ thin films, Thin Solid Films 515 (2006) 2726.

[26] H. Sim, H. Choi, D. Lee, M. Chang, D. Choi, Y. Son, E.H. Lee, W. Kim, Y. Park, I.K. Yoo, H. Hwang, Excellent resistance switching characteristics of Pt/SrTiO3 schottky junction for multi-bit nonvolatile memory application, in: IEDM Tech. Dig., 2005, pp. 777–780.

[27] S. Seo, M.J. Lee, D.C. Kim, S.E. Ahn, B.-H. Park, Y.S. Kim, I.K. Yoo, I.S. Byun, I.R. Hwang, S.H. Kim, J.-S. Kim, J.S. Choi, J.H. Lee, S.H. Jeon, S.H. Hong, B.H. Park, Electrode dependence of resistance switching in polycrystalline NiO films, Appl. Phys. Lett. 87 (2005) 263507.

[28] C.Y. Lin, C.Y. Wu, C.Y. Wu, T.C. Lee, F.L. Yang, C. Hu, T.Y. Tseng, Effect of top electrode material on resistive switching properties of ZrO_2 film memory devices, IEEE Electron Device Lett. 28 (2007) 366–368.

[29] S.Y. Wang, D.Y. Lee, T.Y. Tseng, C.Y. Lin, Effects of Ti top electrode thickness on the resistive switching behaviors of rf-sputtered ZrO_2 memory films, Appl. Phys. Lett. 95 (2009) 112904.

[30] D. Berco, T.Y. Tseng, A numerical study of forming voltage and switching polarity dependence on Ti top electrode thickness in ZrO_2 RRAM, J. Comput. Electron. 15 (2016) 595–601.

[31] D.C. Gilmer, S. Koveshnikov, B. butcher, G. Bursuker, A. Kalantarian, M. Sung, R. Geer, Y. Nishi, P. Kirsch, R. Jammy, Superior filament formation control in HfO_2 based RRAM for high performance low power operation of 1 μA to 20 μA at +/− 1 V, in: IEEE Proceedings of Technical Program of 2012VLSI Technology, System and Application, 2012, pp. 1–2.

[32] U. Chand, K.C. Huang, C.Y. Huang, T.Y. Tseng, Mechanism of nonlinear switching in HfO_2- based crossbar RRAM with inserting large bandgap tunneling barrier layer, IEEE Trans. Electron. Devices 62 (2015) 3665–3670.

[33] D.Y. Lee, T.L. Tsai, T.Y. Tseng, Unipolar resistive switching behavior in Pt/HfO_2/TiN device with inserting ZrO_2 layer and its 1 diode –1 resistor characteristics, Appl. Phys. Lett. 103 (2013) 032905.

[34] H.Y. Lee, P.S. Chen, T.Y. Wu, Y.S. Chen, F. Chen, C.C. Wang, P.J. Tzeng, C.H. Lin, M.J. Tsai, C. Lien, HfOx bipolar resistive memory with robust enduranceusing AlCu as buffer electrode, IEEE Electron. Device Lett. 30 (2009) 703–705.

[35] C.Y. Huang, C.Y. Huang, T.L. Tsai, C.A. Lin, T.Y. Tseng, Switching mechanism of double forming process phenomenon in ZrO_x/HfO_y bilayer resistive switching memory structure with large endurance, Appl. Phys. Lett. 104 (2014) 062901.

[36] C. Walczyk, D. Walczyk, T. Schroeder, T. Bertaud, M. Sowinska, M. Lukosius, M. Fraschke, D. Wolansky, B. Tillack, E. Miranda, C. Wenger, Impact of temperature on the resistive switching behavior of embedded HfO_2- based RRAM devices, IEEE Trans. Electron. Devices 58 (2011) 3124–3131.

[37] R. Fang, W. Chen, L. Gao, W. Yu, S. Yu, Low- Temperature characteristics of HfO_x based resistive random access memory, IEEE Trans. Electron. Devices 36 (2015) 567–569.

[38] T.L. Tsai, h.Y. Chang, F.S. Jiang, T.Y. Tseng, Impact of post oxide deposition annealing on resistive switching in HfO_2- based oxide RRAM and conductive bridge RRAM devices, IEEE Electron. Device Lett. 36 (2015) 1146–1148.

[39] C.Y. Huang, Y.T. Ho, C.J. Hung, T.Y. Tseng, Compact Ga-doped ZnO nanorod thin film for making high-performance transparent resistive switching memory, IEEE Trans. Electron. Device 61 (2014) 3435–3441.

[40] Y.S. Chen, H.Y. Lee, P.S. Chen, P.Y. Gu, C.W. Chen, W.P. Lin, W.H. Liu, Y.Y. Hsu, S. S. Sheu, P.C. Chiang, W.S. Chen, F.T. Chen, C.H. Lien, M.-.J. Tsai, Highly scalable hafnium oxide memory with improvements of resistive distribution and read disturb immunity, in: Tech. Dig. IEEE International Electron Devices Meeting, 2009, pp. 95–98.

[41] B. Govoreanu, G.S. Kar, Y. Chen, V. Paraschiv, S. Kubicek, A. Fantini, I.P. Radu, L. Goux, S. Clima, R. Degraeve, N. Jossart, O. Richard, T. Vandeweyer, K. Seo, P. Hendrickx, G. Pourtois, H. Bender, L. Altimime, D.J. Wouters, J.A. Kittl, M. Jurczak, 10×10 nm^2 Hf/HfO_x crossbar resistive RAM with excellent performance, reliability and low-energy operation, in: Tech. Dig. International Electron Device Meeting, Washington, 2011, pp. 729–732.

[42] C. Nguyen, C. Cagli, E. Vianello, A. Persico, G. Molas, G. Reimbold, Q. Rafhay, G. Ghibaudo, Advanced 1T1R test vehicle for RRAM nanosecond range switching-time resolution and reliability assessment, in: 2015 IEEE Int. Integrated Reliability Workshop (IIRW), 15, 2015, pp. 17–20.

[43] D. Garbin, E. Vianello, O. Bichler, Q. Rafhay, C. Gamrat, G. Ghibaudo, B. DeSalvo, L. Perniola, HfO_2-Based OxRAM devices as synapses for convolutional neural networks, IEEE Trans. Electron Devices 62 (2015) 2494–2501.

View publication stats